Journal of
Mechanics of
Materials and Structures

SPECTRAL ELEMENT APPROACH TO WAVE PROPAGATION IN UNCERTAIN BEAM STRUCTURES

V. Ajith and S. Gopalakrishnan

Volume 5, No. 4 April 2010

mathematical sciences publishers

JOURNAL OF MECHANICS OF MATERIALS AND STRUCTURES
Vol. 5, No. 4, 2010

SPECTRAL ELEMENT APPROACH TO WAVE PROPAGATION IN UNCERTAIN BEAM STRUCTURES

V. AJITH AND S. GOPALAKRISHNAN

This paper presents a study on the uncertainty in material parameters of wave propagation responses in metallic beam structures. Special effort is made to quantify the effect of uncertainty in the wave propagation responses at high frequencies. Both the modulus of elasticity and the density are considered uncertain. The analysis is performed using a Monte Carlo simulation (MCS) under the spectral finite element method (SEM). The randomness in the material properties is characterized by three different distributions, the normal, Weibull and extreme value distributions. Their effect on wave propagation in beams is investigated. The numerical study shows that the CPU time taken for MCS under SEM is about 48 times less than for MCS under a conventional one-dimensional finite element environment for 50 kHz loading. The numerical results presented investigate effects of material uncertainties on high frequency modes. A study is performed on the usage of different beam theories and their uncertain responses due to dynamic impulse load. These studies show that even for a small coefficient of variation, significant changes in the above parameters are noticed. A number of interesting results are presented, showing the true effects of uncertainty response due to dynamic impulse load.

1. Introduction

In the last few years, we have witnessed great improvement in the area of new material research. As a result there is a rapid growth in the use of lighter materials in aerospace and other major industries. These materials show significant variation in material properties and as a result, create a variety of structural problems in which the uncertainties in these properties play a major part in design. Uncertainties may exist in the characteristics of the structure itself and in the environment to which the structure is exposed [Vinckenroy and De Wilde 1995]. The lack of knowledge of material properties and their behaviors can be categorized as the first type of uncertainty. The other type of uncertainty is due to the change in the load and support condition with the change in environmental variables such as temperature and pressure. Another important aspect, when considering the sources of uncertainties, is the modeling technique. In this context, when the variability is large, we can find in the literature that the probabilistic models are more advantageous than the deterministic ones. In probabilistic methods, uncertainty in the parameters is considered and is represented by a random variable or random field. Development in the field of computers has revolutionized the status of research in this area [Li and Chen 2006]. In many cases of structural design, with the availability of computational tools such as Monte Carlo simulations, uncertainty analysis is incorporated in the design phase of the structures.

Keywords: MCS, SEM, normal distribution, Weibull distribution, extreme value distribution, wavenumber, group speeds.
Work supported by the Boeing Aircraft Company (Chicago, IL). The authors are thankful to Mr. Edward White of Boeing for valuable suggestions.

One of the major divisions in the field of probabilistic methods in mechanics is between statistical and nonstatistical approaches [Liu et al. 1986a]. Direct Monte Carlo simulation (MCS), which involves sampling and estimation, is an example of a frequently used statistical approach; the theory of MCS is explained in [James 1980; Decker 1991; Schueller 2001]. Techniques like the random perturbation method, orthogonal polynomial expansion methods, and numerical integration come under the category of nonstatistical schemes [Li and Chen 2006]. Nonstatistical methods do not need prior knowledge about the multivariate distribution of the stochastic parameters. Because of their simplicity and low computational effort, perturbation techniques are used along with the stochastic finite element method (PSFEM) in many problems in static and dynamic elastic analysis, composite ply failure problems, inelastic deformation studies, analysis of free vibration of composite cantilevers, and nonlinear dynamics [Kleiber and Hien 1992]. The simplicity and low computational cost makes PSFEM advantageous. However, in this approach, because of the use of Taylor series expansion for the approximation of the structural response, accurate results are expected only for the case of low variability of the parameters and for nearly linear problems. The method of orthogonal expansion is also used widely for a variety of structural problems [Ghanem and Spanos 2003]. In this method, the accuracy is highly influenced by the variability of parameters and the linearity of the problem. From the literature [Liu et al. 1986a; Liu et al. 1986b; Li and Chen 2006], we see the inability of the nonstatistical approaches to handle large variances of the random variables when compared with their mean values. Usually, the maximum bound set for the coefficient of variation (COV) is 10%. However, some researchers [Ang and Tang 1975; Liu et al. 1986b] have shown that acceptable results can be obtained even if the COV is as high as 20%. The Monte Carlo method is a versatile approach, which can be applied easily to any complex problem whose deterministic solution is known [Shinozuka 1972; Spanos and Zeldin 1998; Lepage 2006]. This method is commonly used for the prediction of the eigenvalues of structures [Lepage 2006]. The Monte Carlo method can be coupled with the finite element method with only slight modification in the parent code. Here the results converge to the correct solution as the number of simulations becomes large and hence the method becomes computationally expensive. Monte Carlo solutions are usually used as reference solutions on account of the absence of inherent assumptions [Cecchi and Sab 2009]. In some literature the Monte Carlo method is used along with other methods to reduce computational time. A compatible blend of the Neumann expansion with MCS has been found to work efficiently for computation of stochastic structural response [Bhattacharyya and Chakraborty 2002]. There are also many methods of sampling available in the literature to improve the accuracy and the efficiency of Monte Carlo methods [Lepage 2006; Stefanou 2009].

In the area of structural health monitoring, wave propagation responses, which are very sensitive to small stiffness changes, are used effectively to detect small defects, such as delamination, cracks, et cetera, in structures [Nag et al. 2003; Ostachowicz 2005; Gopalakrishnan et al. 2008]. However, structures made from common structural materials exhibit large variation in material properties. The response to dynamic loading shows significant changes in responses compared to the deterministic value. The presence of damage causes stiffness reduction, which causes a shift in the natural frequencies, especially at high frequencies [Pardoen 1989]. Variation in the material properties also shifts the natural frequencies and the modal amplitudes. Without a proper uncertain dynamic analysis, these shifts in natural frequencies can be misunderstood as being caused by the presence of structural damage. The deterministic wave propagation analysis in such cases will give results which may be misleading. Hence, a detailed study on the effect of variation in the different structural parameters on the structural response, for a high

frequency impact load, is required to bring greater clarity to the interpretation of the obtained results. However, to the author's best knowledge not much work has been done in the area of uncertainties in wave propagation in structures. Also, high frequency response analysis using the conventional finite element method is computationally expensive since the maximum possible size of the finite element depends on the wavelength of the propagating wave [Horr and Safi 2003; Gopalakrishnan et al. 2008]. Consequently, some of the current literature on the high frequency analysis of structural response uses the spectral finite element method (SEM) [Gopalakrishnan et al. 2008], which combines the accuracy of conventional spectral methods and the geometric flexibility of finite element methods. Unlike the spectral methods in PSFEM, the solution from SEM is exact in most of the deterministic case [Doyle 1997; Gopalakrishnan et al. 2008]. Also SEM, due to its ability to model the inertial distribution of the structure accurately, requires a very small system size to model and obtain deterministic responses, especially for high frequency content loads. The speed of wave analysis using SEM depends on the total time window required to avoid the problems due to enforced periodicity; the time window can be adjusted by changing the time sampling rate or the number of FFT points. The increase in the group speed with frequency reduces the total time window needed for the analysis, which further reduces the computational time. However, in conventional FEM, the requirement that the size of the element be comparable with the wavelength makes the problem size so large that it becomes computationally prohibitive, especially in the context of uncertainty analysis. Large computational times are the major restricting factor for researchers in performing high frequency wave propagation analysis in an uncertain environment. In this context the reduction in computational time of SEM and the large increase in its computational efficiency over conventional FEM with increase in frequency is a very relevant fact, and still an unexplored area of research. Incorporating MCS under SEM is straightforward. Due to its very small size, incorporation of MCS under SEM, unlike conventional FEM, can no longer be considered a luxury from the computational viewpoint. MCS under SEM can be part of the design. The versatility of the Monte Carlo approach and the time aspect of SEM are the major factors which paved the way for the union of these two approaches. This will help researchers to save an immense amount of computational time, especially in the field of uncertain wave propagation analysis.

The paper is organized as follows. In Section 2, a brief description of conventional SEM is given, which is followed by the brief description of MCS and the implementation of SEM under MCS. Section 3 details numerical examples. First we conduct a study on the effects of uncertainties on the time domain responses. Then the computational superiority of SEM under MCS, as opposed to conventional FEM under MCS, is established. Then uncertainty analysis is performed for the frequency response functions. In Section 4A we analyze the variation of time of arrival of first reflection with uncertainty, which is followed by a study of the effect of loading frequency (for a tone-burst signal) on the uncertain responses and a detailed study on spectrum relations. It is well known that the inclusion of higher-order effects dramatically changes the deterministic response in an elementary beam and rod. Hence, a small subsection is included on the effects of different beam and rod theories on the uncertain responses. In all cases, both the Young's modulus and density of structure are considered as uncertain, with their statistical distributions assumed as normal, Weibull, and extreme value distributions. In addition, in most cases both axial and bending responses are considered to study the effects of uncertainties, where the load histories considered are broad-band triangular loading and narrow-band, modulated tone-burst loading. We present some interesting results on the input and output distributions of these parameters.

2. The spectral finite element method

In the spectral element approach, the actual response is synthesized by a prudent combination of many infinitely long wave trains of different periods (or frequencies). Thus the governing equations are first converted to the frequency domain using discrete Fourier transforms and solved. The last step of the analysis involves performing an inverse Fourier transform to reconstruct the signal to obtain the time domain responses. In SEM, the stiffness matrix is established in the frequency domain, which is the main difference between it and conventional FEM. Also in contrast to conventional FEM, the spectral elements can span all the way from one joint. Hence, SEM yields system sizes many orders smaller than for conventional FEM. More details of this approach are given in [Gopalakrishnan et al. 2008]. In this section, we briefly discuss the formulation of spectral rod and beam element formulation. In the case of beams, we provide the formulation of both Euler–Bernoulli and Timoshenko beam, although only the Timoshenko beam model is used in all simulations.

For a rod [Gopalakrishnan et al. 2008], the governing partial differential equation is

$$EA\frac{\partial^2 u}{\partial x^2} - \rho A\frac{\partial^2 u}{\partial t^2} = 0, \tag{2-1}$$

where $u(x, t)$ is the axial displacement, ρ the density, E the Young's modulus, and A the cross sectional area. In SEM the common procedure is to convert this governing partial differential equation to the frequency domain and to solve the ordinary differential equations so obtained. This is a discrete Fourier transform (DFT) based analysis of wave propagation, where the DFT is performed by a FFT algorithm, popularly known as a Cooley–Tukey algorithm [Doyle 1997; Gopalakrishnan et al. 2008]. The DFT of u is given as a solution in exponential form:

$$u(x, t) = \sum_{n=1}^{N} \hat{u}_n(x, \omega_n) e^{i\omega_n t}, \tag{2-2}$$

where $\hat{u}_n(x, \omega_n)$ is the transform of $u(x, t)$, N is the number of FFT points, and ω_n is the frequency at the n-th sampling point.

Substitution of (2-2) in (2-1) converts the governing PDE to an ODE:

$$\frac{\partial^2 \hat{u}_n}{\partial x^2} + k_n^2 \hat{u}_n = 0, \tag{2-3}$$

where k_n is the wavenumber, which is given by

$$k_n = \omega_n \sqrt{\frac{\rho A}{EA}}. \tag{2-4}$$

The nature of the wavenumber depends on the frequency, and tells about the type of wave generated by the medium. In the present case, the wavenumber varies linearly with the frequency and hence the waves are nondispersive, that is, they retain their shape as they propagate. The group speed of propagation is obtained from

$$C_g = \frac{d\omega}{dk} = \sqrt{\frac{E}{\rho}}. \tag{2-5}$$

The solution of (2-3) is given by

$$u(x,t) = \sum_{n=1}^{N} [Ae^{-ik_n x} + Be^{+ik_n(L-x)}]e^{i\omega_n t}. \tag{2-6}$$

SEM uses (2-6) as an interpolating function for finite element formulation. The procedure for element formulation, assembly, and solution is similar to that for finite elements and hence is not reported here.

In the case of beams we derive the spectral solution for Euler–Bernoulli beams. The governing equation is given by

$$EI\frac{\partial^4 w}{\partial x^4} = \rho A\frac{\partial^2 w}{\partial t^2}, \tag{2-7}$$

where $w(x,t)$ is the transverse displacement, EI is the flexural rigidity, ρ is the density, and A is the cross sectional area. Transforming (2-7) into the frequency domain using a DFT, we get

$$w(x,t) = \sum_{n=1}^{N} \hat{w}_n(x,\omega_n)e^{i\omega_n t}, \qquad \frac{d^4\hat{w}_n}{dx^4} + k_n^4 = 0, \quad k_n^2 = \sqrt{\frac{\omega_n^2\rho A}{EI}}. \tag{2-8}$$

$\hat{w}(x,\omega_n)$ is the transform of $w(x,t)$. We see that the wavenumber is a nonlinear function of frequency and hence the waves are highly dispersive. Hence the group speed C_g in the case of beams, unlike the case of rods, is a function of frequency, which is a characteristic of the most dispersive waves:

$$C_g = \frac{d\omega}{dk} = 2\sqrt{\omega_n}\left(\frac{EI}{\rho A}\right)^{1/4}. \tag{2-9}$$

Similarly, in Timoshenko beam theory the value of the wavenumber can be calculated from the transformed homogeneous differential equation in the frequency domain [Gopalakrishnan et al. 2008]:

$$GAK\left(\frac{d^2\hat{w}}{dx^2} - \frac{d\hat{\phi}}{dx}\right) + \rho A\omega_n^2\hat{w} = 0, \qquad EI\frac{d^2\hat{\phi}}{dx^2} + GAK\left(\frac{d^2\hat{w}}{dx^2} - \hat{\phi}\right) + \rho I\omega_n^2\hat{\phi} = 0, \tag{2-10}$$

and the boundary conditions

$$(\hat{w}) \text{ or } \left(\hat{V} = GAK\left(\frac{\partial\hat{w}}{\partial x} - \hat{\phi}\right)\right), \qquad (\hat{\phi}) \text{ or } \left(\hat{M} = EI\frac{\partial\hat{\phi}}{\partial x}\right), \tag{2-11}$$

where $\hat{w}(x,\omega_n)$ is the transform of transverse displacement, $\hat{\phi}(x,\omega_n)$ is the transform of slope, G is the modulus of rigidity, A is the cross sectional area, I is the moment of inertia, ω_n is the frequency at the n-th sampling point, ρ is the density, E is the Young's modulus, $\hat{V}(x,\omega_n)$ is the transform of shear force, $\hat{M}(x,\omega_n)$ is the transform of the bending moment, and K is the shear correction factor (K is assumed to have value 0.86 as in [Gopalakrishnan et al. 2008]. Thus from the homogeneous differential equations and the boundary condition we arrive at the characteristic equation for wavenumber computation:

$$[GAKEI]k^4 - [GAK\rho I\omega_n^2 + EI\rho A\omega_n^2]k^2 + [\rho I\omega_n^2 - GAK]\rho A\omega_n^2 = 0. \tag{2-12}$$

Since the equation is of fourth order, we have four solutions for the wavenumber. The second wavenumber, which is associated with shear deformation, is evanescent to start with and becomes propagating at some high frequencies. The frequency at which this happens is called the cutoff frequency,

which is obtained by setting the last term in (2-12) to zero:

$$\omega_c = \sqrt{\frac{GAK}{\rho I}}. \tag{2-13}$$

Elementary beam equations can be obtained by setting GAK to infinity and ρI to zero. Then the complete solution can be written in the form

$$v(x,t) = \sum \left(R_1 e^{-ik_1 x} + R_2 e^{-ik_2 x} - R_1 e^{-ik_1(L-x)} - R_2 e^{-ik_2(L-x)}\right) e^{i\omega_n t}, \tag{2-14}$$

$$\phi(x,t) = \sum \left(A e^{-ik_1 x} + B e^{-ik_2 x} + C e^{-ik_1(L-x)} + D e^{-ik_2(L-x)}\right) e^{i\omega_n t}. \tag{2-15}$$

A, B, C, and D are coefficients determined from the boundary conditions and the R_i are the amplitude ratios given in [Gopalakrishnan et al. 2008]:

$$R_i = \frac{ik_i GAK}{GAKk_i^2 - \rho A\omega_n^2}. \tag{2-16}$$

Note that the Euler–Bernoulli beam predicts unrealistic speeds at higher frequencies. When the beams are thick, the effects of shear are significant, converting the evanescent mode of the Euler–Bernoulli beam to a shear propagating at high frequency. If this mode is not represented properly, then it will lead to erroneous description of the dynamics of the beam. Hence all simulations in the paper are carried out using the Timoshenko beam model.

In the case of the higher-order rod model, in addition to axial deformation, we add the lateral motion through a term associated with the Poisson's contraction. This theory, called Mindlin–Hermann theory, was first formulated for circular cross sections in Mindlin and Herrmann [1952] and later extended to rectangular cross sections in Martin et al. [1994], for metallic structures. The details of the element formulation, wavenumber, and the group speed computation are given in [Martin et al. 1994]. Here, for the sake of completeness, we provide the characteristic equation for computation of the wavenumber:

$$\begin{aligned}\left(2G(1+\bar{\nu})K_1 GI\right)k^4 - \left((2GA)^2(1+2\bar{\nu}) - 2GA(1+\bar{\nu})K_2\rho I\omega_n^2 - K_1 GI\rho A\omega_n^2\right)k^2 \\ + \left(\rho I K_2 \rho I\omega_n^4 - 2GA(1+\bar{\nu})K_2\rho I\omega_n^2\right) = 0,\end{aligned} \tag{2-17}$$

where $\bar{\nu}$ is the effective Poisson's ratio,

$$\bar{\nu} = \frac{\nu}{1-\nu} \tag{2-18}$$

for plane stress problems and

$$\bar{\nu} = \frac{\nu}{1-\nu^2} \tag{2-19}$$

for plane strain problems, where ν is the Poisson's ratio. K_1 and K_2 are correction factors intended to compensate for the approximate form of the displacement field. In this study K_1 and K_2 are assumed to have values 1.2 and 1.75 as in [Martin et al. 1994].

Unlike the elementary rod, the wavenumber is highly dispersive, especially at high frequencies. The lateral contraction mode becomes propagating only at high frequencies. The cutoff frequency occurs at

$$\omega_c = \sqrt{\frac{2GA(1+\bar{\nu})}{\rho I K_2}}. \tag{2-20}$$

3. MCS under SEM

MCS is capable of giving accurate solutions for any problems whose deterministic solution is known, since it statistically converges to the correct solution provided that a large number of simulations are employed. In direct MCS, the procedure starts with the generation of sampling of the input parameters according to their probability distributions and correlations. For each input sample, a deterministic spectral finite element analysis is performed, giving an output sample. Finally, a response sampling is obtained, from which the mean and the standard deviation of the response can be obtained.

The estimator of the response $\bar{y}$ is defined in [Lepage 2006]:

$$\bar{y} = \frac{1}{n} \sum_{i=1}^{n} y_i, \tag{3-1}$$

where n is the number of samples and y_i is the response corresponding to the i-th input sample.

$$E[\bar{y}] = \mu_y \tag{3-2}$$

and

$$\text{var}(\bar{y}) = E[(\bar{y} - E[\bar{y}])^2] = \frac{\sigma_y^2}{n}, \tag{3-3}$$

where $E[\bar{y}]$ and $\text{var}(\bar{y})$ are the expected value (first moment) and variance (second moment) of the random variable and $\mu_y = E[y]$ and $\sigma_y^2 = E[(y - \mu_y)^2]$ denote the unknown mean and variance of the response. In most of the uncertainty analysis the scatter of the distribution is measured in terms of a parameter, the coefficient of variation (COV), which is the ratio of the square root of the variance of the samples to the mean of the samples. The square root of the variance is also called the standard deviation. In this study, we use the COV as a measure of the scatter of the distribution, is COV. COV of an output parameter can also be used to measure the sensitivity of the input parameter by computing the ratio of output COV to input COV. Many such studies are carried out in this paper by considering wave parameters such as wavenumber, speed, cutoff frequency, et cetera, as output parameters and then investigating sensitivity to the material properties.

In wave propagation analysis, this y can be the transform of the time response of axial and transverse velocity, frequency response functions (FRF), wavenumber, group speed, et cetera. Each value of y_i is obtained using deterministic spectral finite element code or by conventional finite element code (for the comparative study) each time.

4. Numerical results and discussions

There are many factors that govern the wave propagation response in a structure. Some of the key factors are the wavenumber, the group speeds, and the natural frequency of vibration and phase information. All the factors depend on the material properties of the medium in which these waves propagate. Since the material properties in this study are considered uncertain, one can expect substantial changes in the wave responses as compared to the deterministic responses. Hence, the aim of this section is to bring in the effects of uncertainty in the material properties on the wavenumbers, group speeds, and natural frequency of the system. The uncertain responses are shown in the form of time histories of velocities, the FRF, or the probability density distribution, in order to bring out clearly the effect of uncertainty in

these parameters. Both broad-band and modulated high frequency tone-burst loading is considered in this study. In particular, the effect of loading frequency on the uncertain response is investigated.

Last but not least, the effect of using higher-order theories on the uncertain response is investigated. It is quite well known [Gopalakrishnan et al. 2008] that higher-order effects in rods and beams manifest themselves in such a manner that introduces the cutoff frequency in the higher-order wave modes, which propagates beyond the cutoff frequency. The cutoff frequency depends on the material properties and geometric properties and occurs at high frequencies. If this cutoff frequency occurs at a frequency which is beyond the point of interest, one can still use the elementary beam model for the analysis. Uncertainty in material properties, geometric properties, or both, can affect its value. Hence, a detailed uncertainty analysis is required, which is undertaken in this section. Here, each result is obtained by the method of MCS coupled with SEM, as discussed in the previous section. In this work the uncertainty is modeled by representing the uncertain parameters by a random variable and by different probability distribution functions to compare the pattern of distribution of the output parameters. Here, the input random variables are created using MATLAB expressions for creating random variables. The spectral elements used for the metallic beams and rods are similar to the type found in [Gopalakrishnan et al. 2008].

First a study of the effect of axial and transverse response of the metallic beam is performed, comparing between conventional FEM and SEM, for a normal distribution and for different COVs of the Young's modulus and the density. Then, variation in the frequency responses, speed, and wavenumber are also analyzed to investigate the variation of these output parameters as discussed previously.

4A. ***Effect of uncertainty on velocity time histories.*** In this study, we consider a cantilever metallic beam 1 m in length with a rectangular cross section of $10\,\text{mm} \times 10\,\text{mm}$. The beam is modeled using a single Timoshenko beam and elementary rod in the SEM case, while 200 one-dimensional beam and rod elements are used in the case of conventional FEM. The deterministic values of the Young's modulus and density are 70 GPa and $2700\,\text{kg}/m^3$ respectively. The objective here is twofold: first we will compare the axial and flexural responses predicted by conventional FEM and SEM to validate the latter; second, we will quantify the responses' changes due to material uncertainties. For the FEM and SEM comparison, we assume only the Young's modulus as uncertain, with a normal distribution. Ten thousand randomly generated samples of the Young's modulus are used in the simulation. In most of the uncertainty analysis, the mean of a parameter obtained from the simulated data should converge to a constant value. This requires a large number of samples; from our study we found that 10,000 samples are required to satisfy this condition. For comparison of the SEM and FEM solutions, two different inputs are used: Figure 1a shows a broad-band loading situation, whose FFT gives a frequency content of 20 kHz. This pulse is used in the case of axial wave propagation. Flexural waves are highly dispersive in nature. This is due to the dependence of the group speeds of the waves on the frequency. One of the ways to make a signal travel nondispersively in a beam is to use a tone-burst modulated pulse, shown in Figure 1b, modulated at a 5 kHz frequency. The FFT of the pulse, shown in the inset of the figure, has significant energy only at 5 kHz, and hence the waves travel at a speed corresponding to 5 kHz. We use this pulse for flexural wave propagation. First we consider the Young's modulus as a random variable and MCS is performed both under conventional FEM and SEM environments using 10,000 samples. Here, in each figure, "min" and "max" signify the minimum and maximum values of the time of arrival of the first reflection obtained through MCS and "det" the value when the material properties are deterministic. Figures 2a and 2b

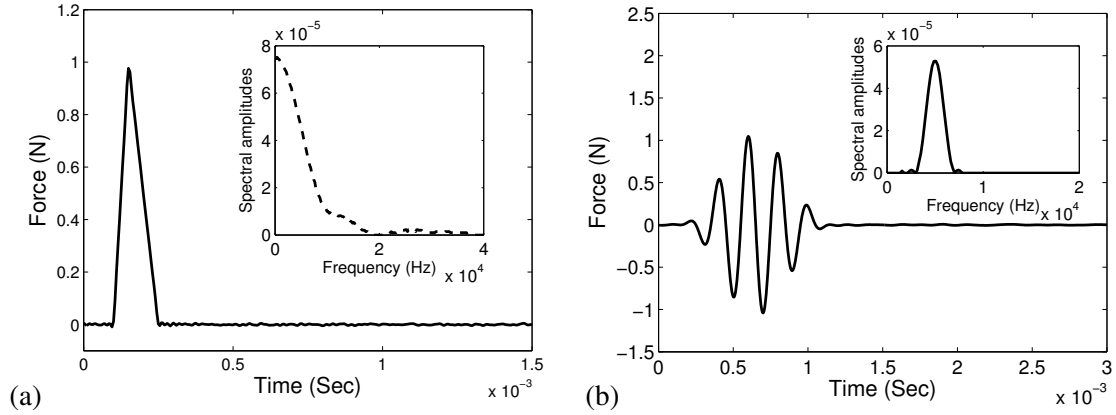

Figure 1. Input force used in simulation: (a) broad-band pulse and (b) narrow band modulated (at 5 kHz) pulse.

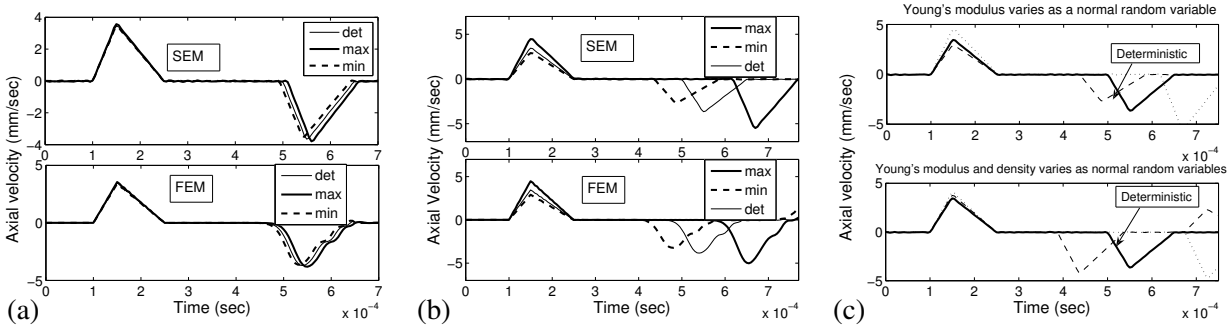

Figure 2. Axial velocity responses: (a) uncertain Young's modulus with COV 1%, (b) uncertain Young's modulus with COV 10%, and (c) uncertain Young's modulus and density with COV 10%.

show the axial velocity histories obtained with input parameters COV 1% and 10% respectively. Two things are quite apparent from the figure. First the predictions made by MCS under FEM and SEM match very well. The second is that if the COV is small, the uncertain response does not deviate much compared to the deterministic response. Since the group speed of the medium depends on the material properties, uncertainty in material properties can cause changes in the predicted group speeds, which can be quantified by looking at the time of arrival of the first reflection. From Figure 2b, it is clear that the total scatter in the time of arrival of the first reflection is 15%, compared to its value in the deterministic case, for a COV of 10%, which in terms of speed will be around 2000 m/s. There is a significant increase in group speed introduced by uncertainties in material properties.

Figures 3a and 3b show the flexural responses obtained through MCS under FEM and SEM as a function of COV. As in the case of axial waves, the FEM and SEM predictions match well. Unlike in the case of axial wave propagation, for larger COVs the scatters induced in the flexural group speeds are not that significant. Next, both Young's modulus and density are made uncertain and we assume a normal distribution for both these parameters. Figures 2c and 3d show, respectively, the axial and transverse velocity histories for the case of 10% COV, obtained through SEM. From these figures, it

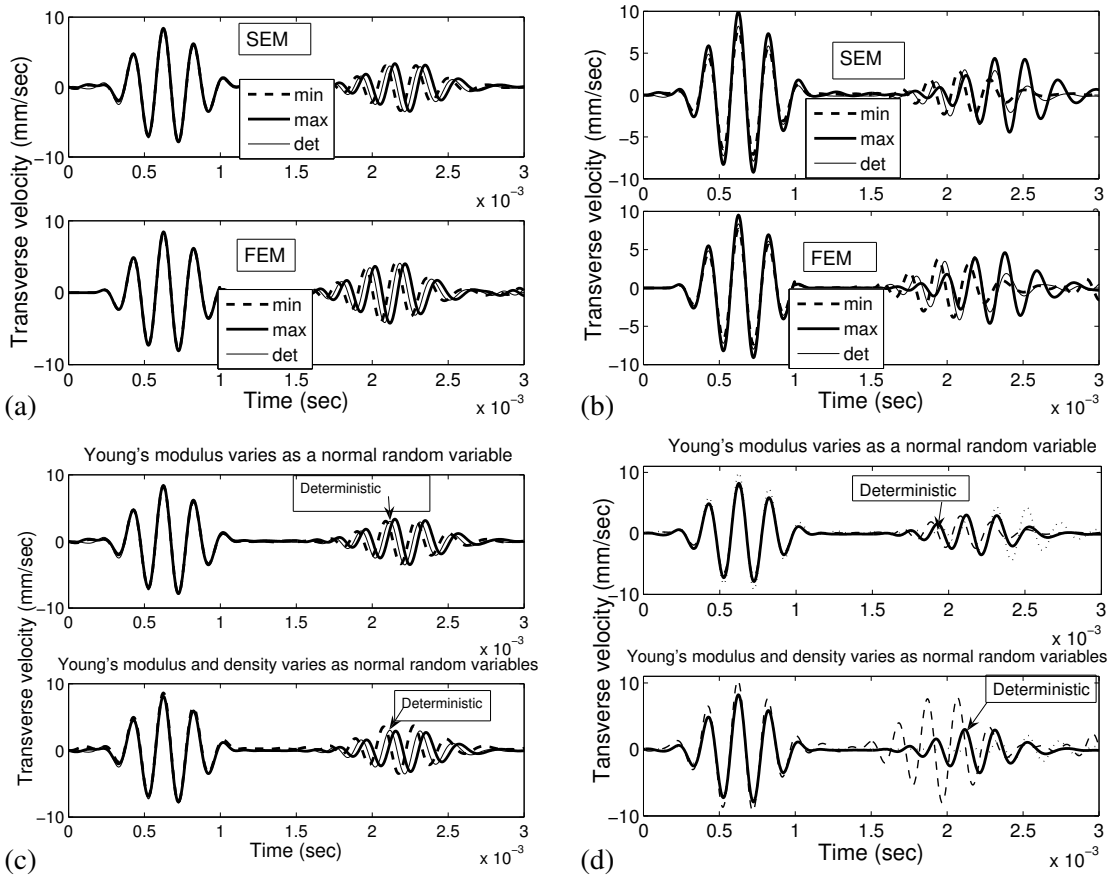

Figure 3. Transverse velocity responses: (a) uncertain Young's modulus with COV 1%, (b) uncertain Young's modulus with COV 10%, (c) uncertain Young's modulus and density with COV 1%, and (d) uncertain Young's modulus and density with COV 10%.

is clear that significant changes in the group speeds are introduced both in the axial and flexural cases, where the total scatters in axial and flexural speeds are about 25% and 20%, respectively when compared to the deterministic responses. In terms of speed, this change amounts to changes in group speeds of 3450 m/s and 350 m/s for the axial and flexural cases, respectively. Figure 3c is the flexural response for a case of COV 1%, from which it can be concluded that the variation in the time responses with the change in the number of input random variables from one to two is significantly less when the COVs of the input parameters are less. In summary, uncertainty in material parameters increases the total scatter in the group speeds. If the modulus alone is uncertain, then the flexural group speeds do not change significantly. However, when both the density and modulus are uncertain, flexural group speeds show a total scatter of nearly 20% with 10% COV in the input parameters. The variation in the time responses with the change in the number of input random variables from one to two is significantly less when the COVs of the input parameters are less.

4B. ***Comparison of efficiency of FEM and SEM using MCS.*** Here, to determine the efficiency of SEM under MCS, the same cantilever beam of the previous example is considered. The beam is modeled as a

single Timoshenko beam. Two different tone-burst loadings, one which samples at 5 kHz and the other at 50 kHz, are used for the study. Figure 4a shows the bending wave speed superimposed on the FFT spectrum of 5 kHz and 50 kHz loading. The 5 kHz load will travel at 1400 m/s while the 50 kHz pulse will travel at 1900 m/s, according to the figure. This means the 50 kHz pulse will travel faster than the 5 kHz loading. Hence, the reflection will arrive earlier under 50 kHz loading, which manifests itself in having a smaller time window compared to the 5 kHz loading. In other words, 50 kHz tone-burst loading needs a smaller time window, which means a smaller number of FFT points, compared to 5 kHz tone-burst loading. Hence, we can expect faster SEM solutions for 50 kHz loading than for 5 kHz loading.

In conventional FEM, when the frequency increases, the wavelength decreases; conventional FEM mandates that the element length should be comparable to its wavelength [Chakraborty and Gopalakrishnan 2004], and typically 6–10 elements should span a wavelength. Hence, increase in loading frequency, increases the problem size in conventional FEM, which will certainly increase the analysis time. This is quite different than the SEM solution. In the present case, increase in the frequency from 5 kHz to 50 kHz

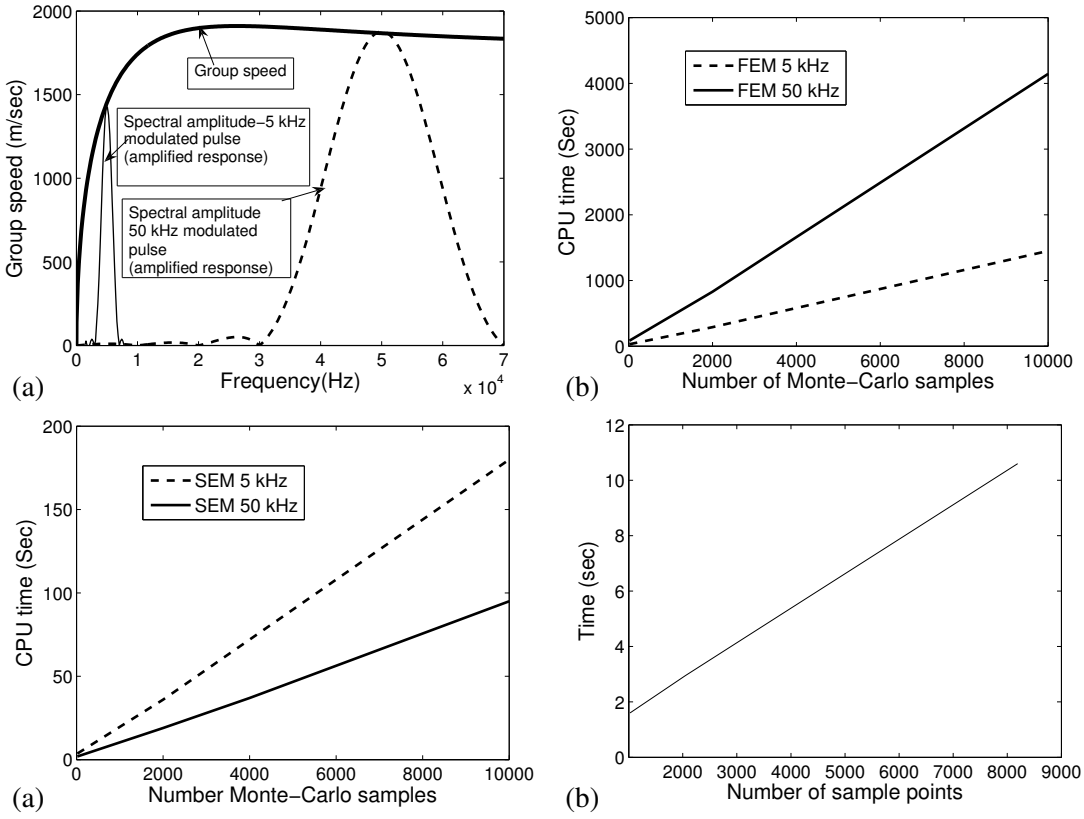

Figure 4. (a) Dispersion plot (bending group speed) of the beam, where the spectral amplitudes (amplitudes are amplified) of 5 kHz and 50 kHz tone-burst signals are superimposed onto it; CPU time as a function of the number of samples for different tone-burst signal frequencies (5 kHz and 50 kHz) with (b) FEM (c) SEM and (d) SEM for different numbers of FFT points for 100 samples.

increases the number of conventional elements required from 200 to 600 elements. Figures 4b and 4c compare the time taken by the MCS under FEM and SEM as a function of number of samples, for the transverse velocity response of a cantilever beam, using two different tone-burst signals. In SEM, a time sampling rate of 5 μs with 1024 FFT points is used for a 5 kHz signal loading; only 512 FFT samples are used for a 50 kHz load. For the conventional FEM we use 200 one-dimensional beam elements for a tone-burst pulse of modulated frequency 5 kHz, and 600 elements for a tone-burst pulse of frequency 50 kHz. Only the Young's modulus is assumed as a random variable; the randomness is modeled as normal distribution. From these figures, we can clearly see that SEM is faster than conventional FEM for both loadings. SEM is 8 times faster for 5 kHz loading and takes less than 200 seconds to compute the responses. The factor increases from 8 to 48 when the frequency content of the load is 50 kHz. Hence, using MCS under SEM cannot be thought of as a luxury.

One of the problems associated with SEM is that it cannot handle finite small dimension structures, which is due to enforced periodicity in the frequency domain used in the DFT. The enforced periodicity causes the responses to wrap around due to its inability to damp out all the responses within the chosen time window. To overcome this, we need to enlarge the time window, which can be done by increasing the time sampling rate, increasing the number of FFT points, or both. In the present case, for a 100 sample MCS simulation, the time taken by SEM as a function of the number of FFT points is shown in Figure 4d. The CPU time variation is linear and quite small. In summary SEM performs the simulations faster than conventional FEM, increasing with the increase in the frequency content of the load.

4C. ***Effect of variation on natural frequencies and modal amplitudes.*** Natural frequencies are functions of the material properties. If these properties are uncertain, then we will see significant variation in the responses predicted by the analysis. In particular, the shift in the natural frequency is used as a way to assess the presence of damage in the structure. There is difficulty in distinguishing the shift in the natural frequency due to damage with the shift in frequency due to material uncertainties, which makes it necessary to perform a detailed uncertainty analysis. SEM directly gives the FRF as a by-product, a plot of which will provide us with insight on how the frequencies are shifting due to material uncertainties.

We first consider a single elementary rod SEM model, fixed at one end. In the first case we consider the Young's modulus alone as uncertain, with its mean value at 70 GPa, and more than 10,000 samples are used in the MCS. In this study we assume only a normal distribution for all the input random variables. Figure 5a shows the FRF for a rod for 1% and 10% COV in the input parameter, the Young's modulus. For 1% COV the shifts in the first three modes are very small; thereafter, there is some increase in the shift. All modes exhibit negligible change in their modal amplitudes. This is also typical behavior of a metallic beam with small cracks. If the COV is increased to 10%, then the fundamental axial modes also change and the shifts in the second and higher frequencies are quite substantial. The changes in modal amplitudes are also significant.

Next, we plot the FRF for axial loading, when both the Young's modulus and density are considered random, as a function of increasing percentage of COV. This is shown in Figure 5b. The notable feature here is that even though the shift in the natural frequency increases drastically the modal amplitudes change little from their deterministic values.

Figures 6a and 6b show the beam FRF, which is modeled as a single Timoshenko beam for the cases of the Young's modulus being random and both the Young's modulus and density being random, respectively.

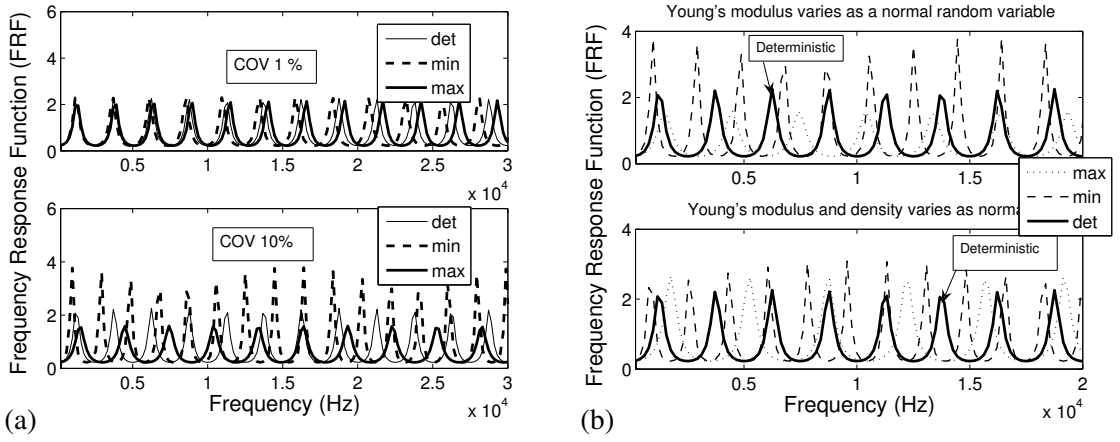

Figure 5. FRF of axial modes for 1% and 10% COV: (a) the Young's modulus is uncertain and (b) both the Young's modulus and density are uncertain (COV 10%).

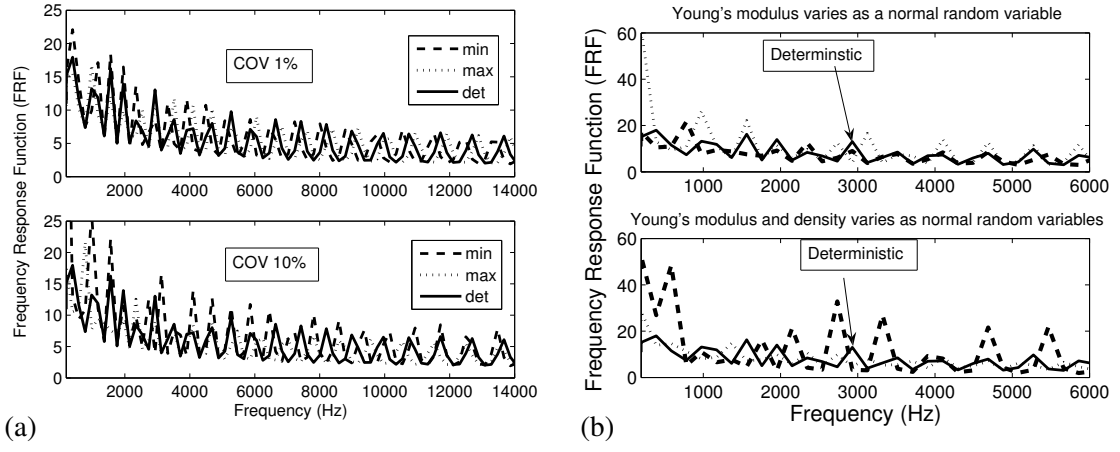

Figure 6. FRF of flexural modes for 1% and 10% COV: (a) the Young's modulus is uncertain and (b) both the Young's modulus and the density are uncertain (COV 10%).

For the case of a random Young's modulus, with 1% COV, as in the case of the rods, there is not much shift in the lower modes. Here, in the case of a beam model, the changes in the fundamental modes and the modal amplitude with the increase in COV to 10% is observed, as in the case of a rod. Figure 6b shows the FRF when both the Young's modulus and density are uncertain for a COV of 10%. When compared to the FRF with only the Young's modulus uncertain, significant shifts are visible for the natural frequencies. However, the modal amplitudes nearly double for most of the modes.

In summary, the frequency shifts for a small COV for both the axial and flexural modes are very small for lower-order modes, while the higher modes exhibit significant shifts. A higher COV not only shows a higher shift for the entire natural frequency spectrum, but also shows higher modal amplitudes.

4D. ***Distribution of time of arrival of first reflection.*** In Section 4A, we showed that the material uncertainties significantly changed the group speeds, where the group speed effects are quantified by computing

the speeds using the time of arrival of the first reflection. In this section, we would like to quantify the group speed changes in terms of the distribution of the time of arrival of the first reflection for two different input material property distributions, namely the normal and extreme value distributions. The extreme value type I distribution based on the smallest extreme values is used in this study, also referred to as the Gumbel distribution. In this case, only a flexural response is considered, where the cantilever beam is modeled as a single Timoshenko element subjected to a point impact load (see Figure 1). As before, 10,000 samples are used in the MCS. The objective here is, for an input COV of material variation, to determine the COV of time of arrival of first reflection.

In each figure, the label "Monte" means that the actual histogram from MCS, while "Normal" and "Extreme" indicate the ideal normal and extreme value distributions with the sample mean and standard deviations obtained from the simulated data. Figure 7 shows the distribution of the time of arrival of the first reflection for two different distributions of the Young's modulus with a COV of 10%. Here, density is assumed to be deterministic. The different input distributions predict similar COVs (about 2.9%) for the output. Next, we assume both the density and Young's modulus as uncertain; these distributions are modeled by normal and extreme value distributions with a COV of 10%. As in the previous case, the COV remains constant (around 3.9%) for the different distributions (Figure 8). For the different distributions, we see that the maximum and minimum limits of the output distribution are not significantly different. In summary, different distribution of material uncertainty does not significantly alter the total bound of variation of the group speed.

4E. ***Effect of loading frequency in time responses with uncertain material properties.*** A tone-burst modulated signal (Figure 1b) is normally used in structural health monitoring studies to detect the presence of cracks in structures since it travels nondispersively. These signals are modulated at certain frequencies, which depend on size of cracks, that is, the smaller the damage, the larger the value of the modulated frequency. The aim of this subsection is to understand and estimate the extend of the shift in the arrival of first reflection that is caused by material uncertainty for an increasing value of loading frequency. In health monitoring studies, this aspect is very critical in order to distinguish clearly the shift in the arrival of first reflection caused by the damage with that caused by the material uncertainties.

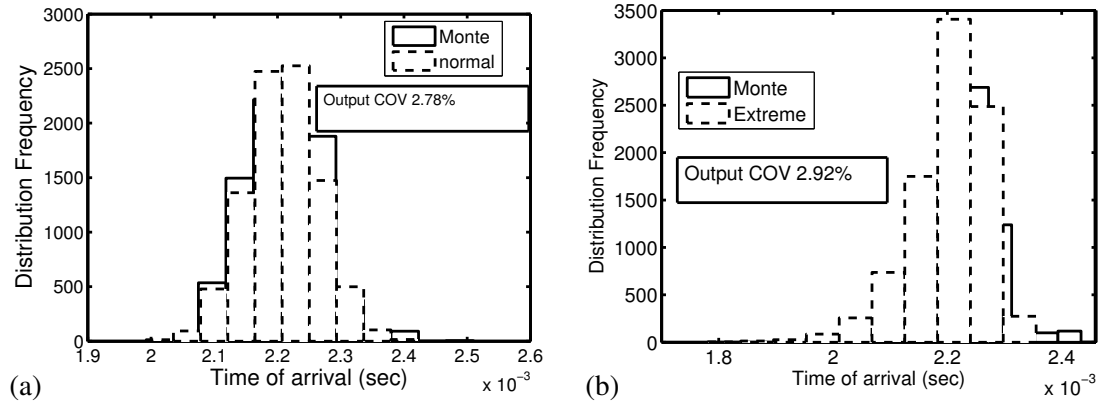

Figure 7. Histogram of distribution of time of arrival of first reflection, Young's modulus with an input COV 10% for different distributions: (a) normal and (b) extreme value.

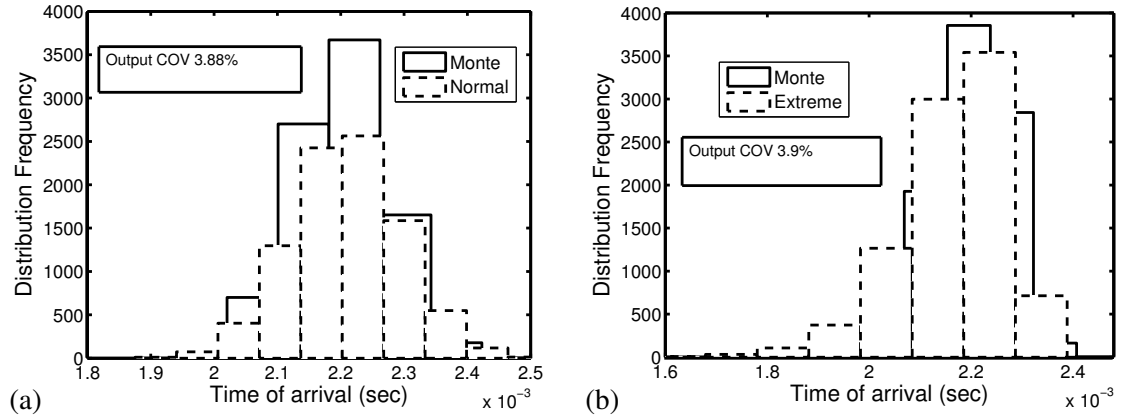

Figure 8. Histogram of distribution of time of arrival for first reflection with uncertain Young's modulus and density with a COV of 10% for different distributions: (a) normal and (b) extreme value.

We again model the same cantilever beam of the previous section with a single Timoshenko beam model and subject this beam to a tone-burst signal (Figure 1b), whose modulated frequencies are varied from 5 kHz to 50 kHz. In each case, results were obtained considering the Young's modulus as uncertain and both the Young's modulus and density as uncertain. In both these cases the COV was fixed at 10%. Figures 9a and 9b show the velocity history responses for frequencies of 20 kHz and 50 kHz, respectively. As in the earlier studies, in both cases the shift in the arrival of the first reflection is maximum when both the Young's modulus and density are uncertain. For 20 kHz loading, the variation in the group speed is about 720 m/s. This variation decreased to 660 m/s for 50 kHz loading. When we quantify these variations in group speed in terms of the percentage of its deterministic value, we can see an increase in the variation of group speed from 27% to 35.5% with the increase in the loading from 5 kHz to 20 kHz. However, for loading with a frequency of 50 kHz, the variation in group speed is about 35.5%. Beyond 50 kHz, we notice no further appreciable change in the group speed. Hence, in health monitoring studies, it is always necessary to use signals modulated at frequencies beyond 50 kHz, if the structure is uncertain, so that the shift in the reflected pulse due to material uncertainties can be factored into the damage location computation.

4F. ***Wavenumber COV for different material property distributions.*** Generally in wave analysis, the wavenumber, which acts as a scale factor on the position variable in the same way that the frequency acts on the time (Equations (2-6), (2-14), and (2-15)), and its variation with frequency are a major areas of study. Uncertainty in the material parameters scatters waves that are very different from the deterministic beam. This scatter will be quite different in the presence of flaws such as cracks, especially when the parameters are uncertain. Two parameters that will help us to differentiate the scattering of waves due to material uncertainties and damage are the wavenumber and group speed of waves. In the application of wave propagation analysis for structural health monitoring, the time of arrival of the first reflection is an important parameter, which directly depends on the group speed of the structure. However, we know that there is a direct relation between wavenumber and group speed, given in (2-5). It is essential to study the variation of wavenumber with the variability of the material properties, which will actually

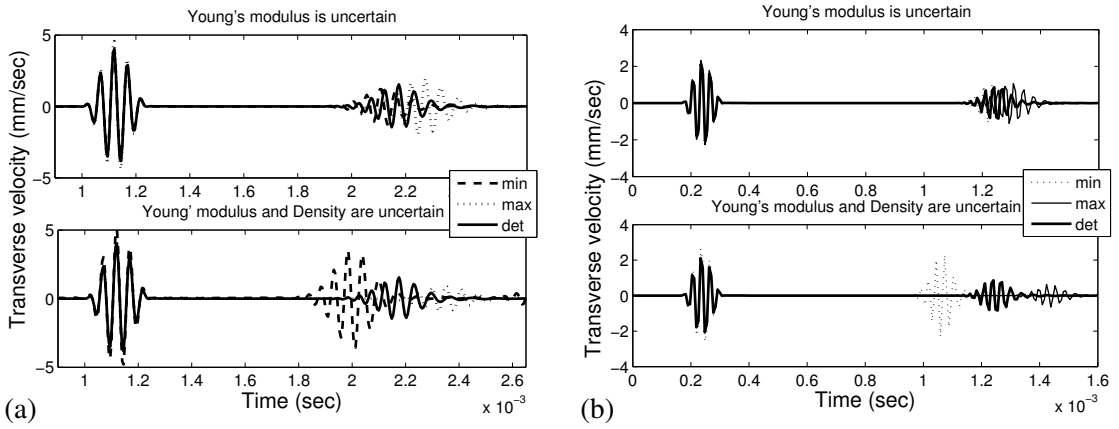

Figure 9. Transverse velocity variation with change in the modulation frequency for (a) 20 kHz loading and (b) 50 kHz loading.

help us in structural health monitoring by giving us insight into the type of variation of group speed and its dependence on the wavenumber. In this study, we try to quantify the variation of COV of the wavenumber with the variation of COV of the input parameters.

Here, we have assumed the material properties (modulus and density) to vary as normal, Weibull, and extreme value distributions. The wave number for the beam is calculated by solving the characteristic equation, (2-12), while for a rod (2-4) is used. As before, 10,000 randomly generated samples are used in the analysis. Figure 10 shows COV plots as a function of a few discrete frequencies for a normal distribution of the material property. From the figure, the following observation can be made. When the Young's modulus alone is uncertain (Figure 10a), the wavenumber COV variation decreases with the increase in frequency; on the other hand, if the density alone is uncertain (Figure 10b), the wavenumber COV variation is just the reverse of the previous case. Figures 11a and 11b show the flexural wavenumber COV variation for a Weibull distribution. These variation patterns follow that of the normally distributed wavenumber COV. No effect of frequency on the COV of wavenumber is noticed in a simple rod and beam model, where the term containing frequency, present in both the denominator and numerator of the expression for the COV, will cancel out. However, in a Timoshenko beam model the frequency has an effect on the variability of the wavenumber, which is explicit from the constant term (the third term) of the characteristic equation (Equation (2-12)). From the above two cases and also from the extreme value distribution of the input parameter, when both the Young's modulus and density are uncertain (Figures 10c, 11b, and 11c), the wavenumber COV is not heavily influenced by the frequency. In fact, compared to the case of a single uncertain input variable, in all these cases the variability in the wavenumber is very high even in the low frequency range, when the Young's modulus and density are uncertain. Figure 12 shows the wavenumber COV for an axial wavenumber. The figures show that the axial wavenumber COV is more than that of a flexural wavenumber COV for a given material distribution and, in contrast to the flexural case, the wavenumber COV does not show any variation with frequency.

4G. ***Distribution of wavenumber, for different types of input distributions.*** In the next few plots, the variation of the wavenumber by taking different probability density functions for the input parameters

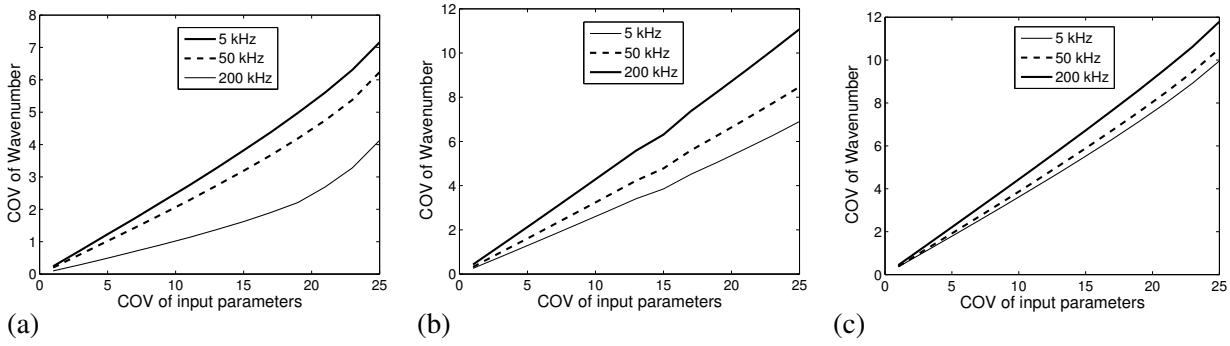

Figure 10. Variation of COV of wavenumber (flexural) with frequency where input parameters vary as normal random variables: (a) Young's modulus, (b) density, and (c) Young's modulus and density.

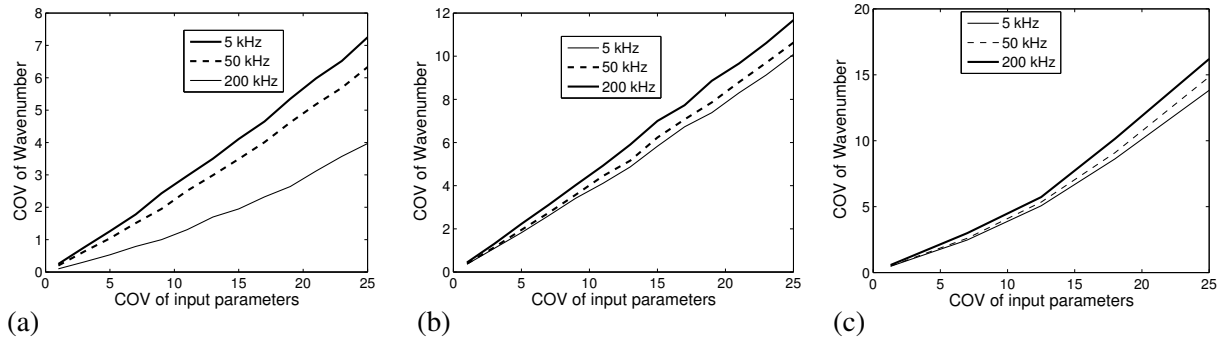

Figure 11. Variation of COV of wavenumber (flexural) with frequency where input parameters are taken as Weibull and extreme value random variables: (a) Young's modulus (Weibull), (b) Young's modulus and density (Weibull), and (c) Young's modulus and density (extreme value distribution).

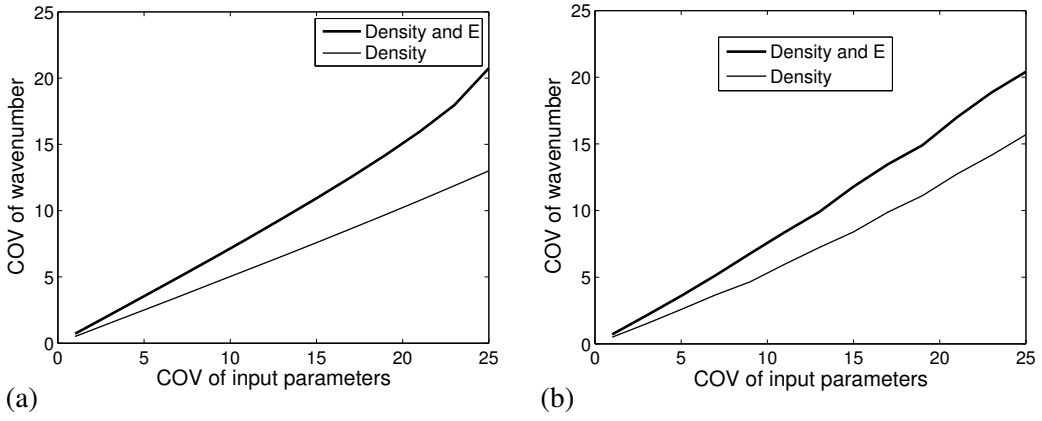

Figure 12. Variation of COV of wavenumber (axial) with input parameters (density and Young's modulus) varying as (a) normal and (b) Weibull random variables.

is shown to quantify the effects of material uncertainty. Here we are only studying the variation in the flexural wavenumber and the uncertain input parameters considered are the Young's modulus and density. Figures 13a and 13b show the change in the variation distribution of the flexural wavenumber at 10 kHz and 25 kHz, taking the input parameters as normal random variables with COV 7%. MCS is performed using 10,000 samples and the corresponding normal distributions of the output samples are obtained using the estimates of the MCS, for purposes of comparison. In Figure 14 the input parameters are taken as Weibull distributions and in Figure 15 the input parameter uncertainty is represented as an extreme value distribution. Here, the different discrete frequencies, where the wavenumber is calculated, are 25 kHz and 200 kHz. Similar to the previous case, the corresponding Weibull and extreme value distributions of the output are obtained using the estimates of the MCS. The results show that the distribution of the variation of the wavenumber at a particular frequency does not vary much with the change in the type

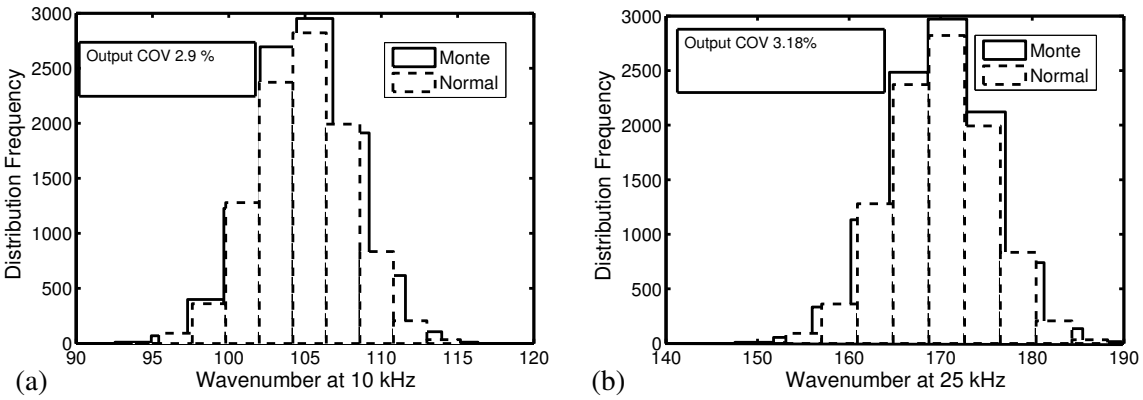

Figure 13. Histogram of distribution of wavenumber (flexural) at different frequencies, with both uncertain density and Young's modulus modeled as normal random variables with COV 7%: (a) 10 kHz and (b) 25 kHz.

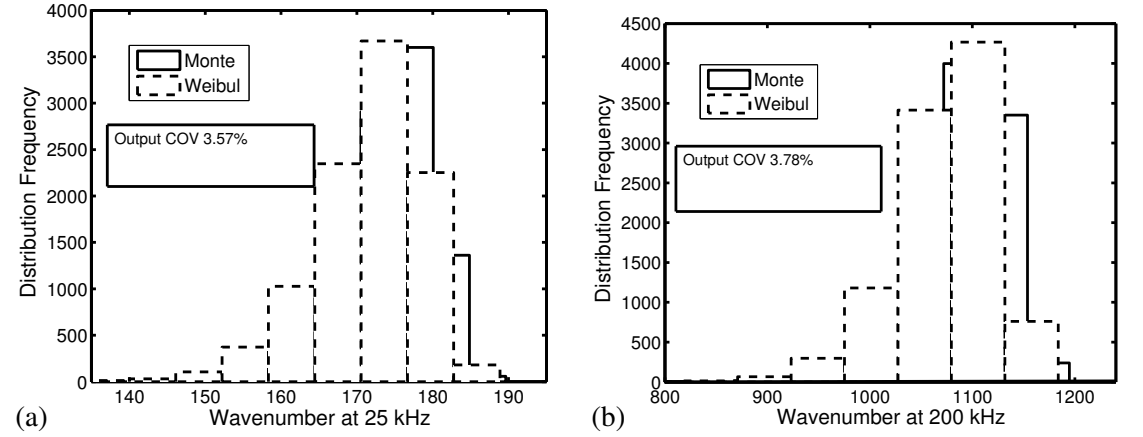

Figure 14. Histogram of distribution of wavenumber (flexural) at different frequencies, with both uncertain density and Young's modulus modeled as Weibull random variables with COV 7%: (a) 25 kHz and (b) 200 kHz.

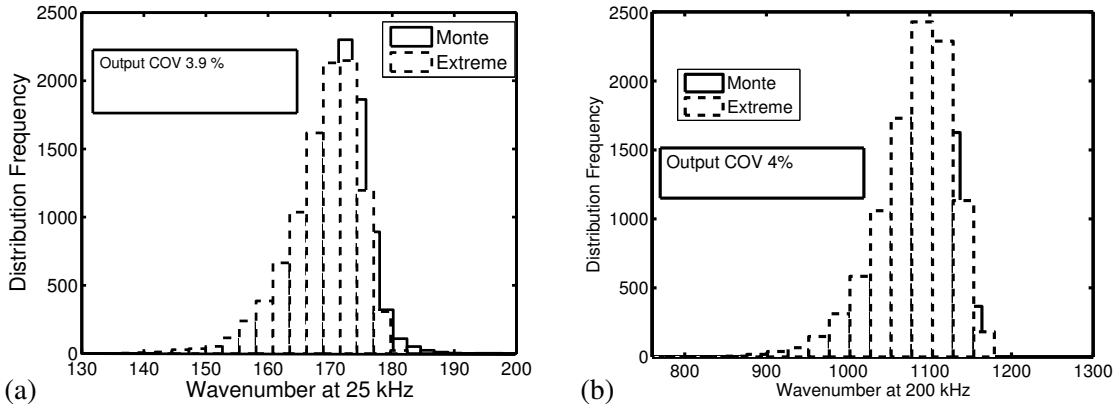

Figure 15. Histogram of distribution of wavenumber (flexural) at different frequencies, with both uncertain density and Young's modulus modeled as extreme value random variables with COV 7%: (a) 25 kHz and (b) 200 kHz.

of probability distribution function. The minimum and maximum limits obtained are similar in all cases, regardless of the type of distribution considered. Moreover, it can be seen that the COV of the variation of the wavenumber does not vary much with the increase in the corresponding frequency.

4H. ***Effect of uncertainty on wavenumber due to higher-order effects in metallic rods and beams.*** In Section 2 we have discussed in detail the computation of the wavenumber. In an elementary rod, there is only one mode due to axial deformation, which is propagating. The wavenumber varies linearly as frequency and hence is nondispersive. This model was used in all earlier simulations. An elementary beam, on the other hand, has a wavenumber which is a nonlinear function of frequency and hence dispersive. It has two modes, one of which is propagating and the other evanescent. Introducing higher-order effects to this elementary model completely alters the wave mechanics. The lateral higher-order effects in rods are introduced by adding an additional lateral motion attributed to the Poisson's ratio. The wavenumber computation for the model is given in Section 2. Higher-order effects introduce an additional propagating mode beyond a certain frequency called the cutoff frequency, which occurs at very high frequencies. In fact, the existence of a cutoff frequency determines the usage of a particular rod model, either an elementary or higher-order model. That is, if the frequency of interest falls below the cutoff frequency, one can still use an elementary model for analysis. Similarly, higher-order effects in beams can be introduced through the introduction of shear deformation, which makes the evanescent mode propagating after a certain cutoff frequency. The cutoff frequency is governed by the material and geometric properties of the structure. In light of the fact that the uncertainties involved in the determination of material properties of a real structure are greater, first we focus our study on the variation of the cutoff frequency of the structure with the variability in the material properties. Here, the geometric properties of the system are considered deterministic, and never initiate higher-order effects in the system. However, if the material properties are uncertain, the predicted cutoff frequencies may be quite misleading in deciding the type of analysis to be used. The aim of this section is to determine the range of shift in the cutoff frequencies due to material uncertainties so that proper theories can be used in the simulation process.

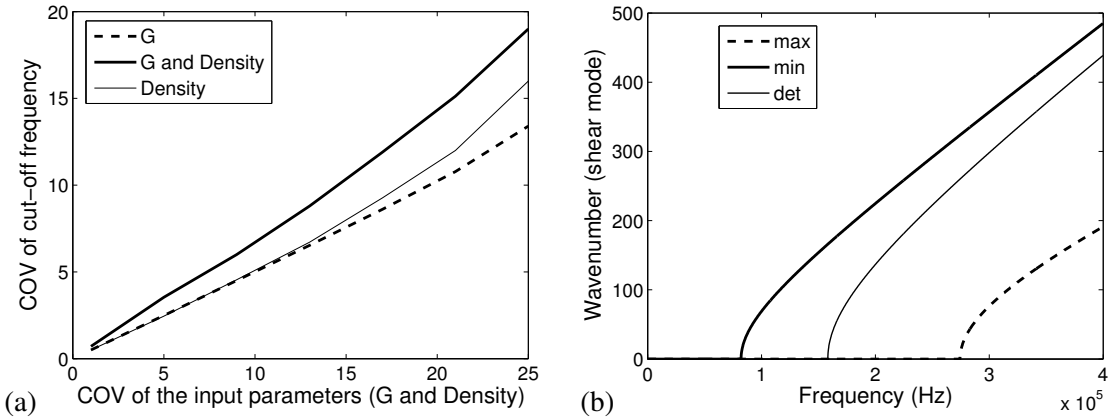

Figure 16. Variation of cutoff frequency of the shear mode of a Timoshenko beam, with both uncertain rigidity modulus and density normal with COV 20%: (a) variation of COV and (b) maximum and minimum bounds of cutoff frequency.

Figure 16a shows the variation of the cutoff frequency with the change in COV of the input parameters (density and G). When the number of random variables used increases from one (density or G) to two (both density and G), we can see that the COV of the cutoff frequency increases. The variation of the COV of the cutoff frequency is greater when the input random variable is density, especially when the COV of the input is high. Figure 16b shows the upper and lower bounds of the shear mode when the COV of the input random variable is 20% and the number of random variables is two (density and G). There is a variation from the deterministic value or 161 kHz to 78 kHz in the lower limit and 271 kHz in the upper limit. The lower limit of this result suggests that, when there is such a large variation in the input parameters, there is a chance for the shear mode to propagate at a lower frequency (here it is 78 kHz) than the expected frequency (161 kHz), which cannot be traced by a simple Euler–Bernoulli theory even for a thin beam. The distributions of the cutoff frequency for different distributions are shown in Figure 17.

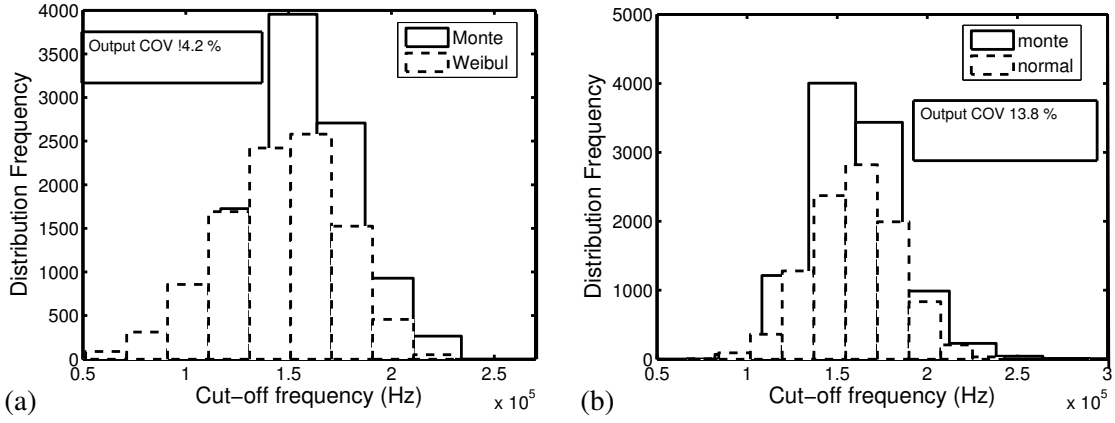

Figure 17. Histogram of the distribution of cutoff frequency of the shear mode of a Timoshenko beam, with both density and rigidity modulus uncertain using different input distributions with COV 20%: (a) normal and (b) Weibull input distribution.

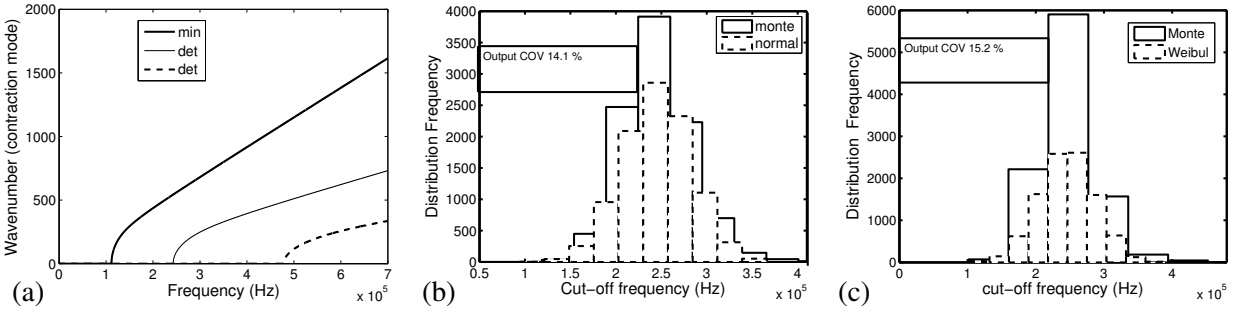

Figure 18. Variation of cutoff frequency for a higher-order rod for uncertain density and rigidity modulus, with COV 20% for different distributions: (a) maximum and minimum limit for normal; histograms of distribution of cutoff frequency for input distributions (b) normal and (c) Weibull.

	Normal		Weibull	
COV (%)	maximum	minimum	maximum	minimum
1	165.74	157.25	158.44	149.02
5	185.48	141.32	173.07	134.35
10	216.86	126.11	198.22	112.34
15	246.62	98.58	223.69	85.24
20	271.24	78.12	245.54	67.33

Table 1. Total bounds on variation of cutoff frequency (kHz) with different input COVs, when both the Young's modulus and density are uncertain, for a Timoshenko beam.

We can see the output distribution variation is almost the same for the two distributions considered and differs from the corresponding input distribution pattern in both cases, where the input parameters are taken as normal distributions and as Weibull distributions.

Figure 18a shows the variation in the contraction mode of a higher-order rod. From this figure, we can see the deterministic value of cutoff frequency for a higher-order rod is very much higher than that for the previous case of a higher-order beam. The uncertain response has the same impact as in the case of the beam in the maximum limit (here, 123 kHz) of frequency of the load, which can be used with the simple elementary rod model. The distribution of the cutoff frequency shows the same pattern of distribution as that of the beam model (Figures 18b and 18c). Finally, Tables 1 and 2 give us an idea of the total bounds on variation of the cutoff frequencies of a Timoshenko beam and a higher-order rod, as a function of the COV of the input parameter, when both the Young's modulus and density are uncertain.

5. Conclusions

Monte Carlo simulation coupled with the spectral finite element method (SEM) is applied to study the variation in the high frequency response of a metallic beam and rod with the variation in the material properties. It can be seen that the method using SEM is efficient and takes much less time than taken by

	Normal		Weibull	
COV (%)	maximum	minimum	maximum	minimum
1	278.66	262.82	280.74	260.47
5	314.21	233.04	327.71	229.84
10	364.65	201.93	395.65	191.93
15	398.69	168.42	423.69	152.42
20	455.38	123.46	495.53	98.34

Table 2. Total bounds on variation of cutoff frequency (kHz) with different input COVs, when both the Young's modulus and density are uncertain, for a higher-order rod.

the method using conventional FEM. The ratio between the CPU time taken for conventional FEM and SEM increases with the loading frequency (here, it increases from 8 to 48 as the frequency content of the load increases from 5 kHz to 50 kHz). Increase in the number of random variables used affects the responses considerably, but only when the coefficient of variation is large. The change in the variation of the time response and the dispersion relations with the increase in the frequency only depends on the uncertain input parameters considered. Regardless of the input parameter distributions considered, the maximum and minimum bounds on the time of first reflection and the wavenumber variation distributions almost match in all the cases. The variation of the shear mode in the beam and the contraction mode in the higher order rod suggest that the uncertainty enforces the use of higher-order theories at lower frequencies than the expected frequency, even for thin structures.

Finally, at this stage, it is very difficult to determine the reason for the shift in the arrival of the first reflection. For understanding the shift due to damage, uncertainties in damage location, size, and type of damage also need to be introduced into the formulation. This is indeed an open area of research and the authors are working towards their next article focusing on this very concept.

References

[Ang and Tang 1975] A. H. S. Ang and W. H. Tang, *Probability concepts in engineering planning and design, vol. 1: Basic principles*, Wiley, New York, 1975.

[Bhattacharyya and Chakraborty 2002] B. Bhattacharyya and S. Chakraborty, "NE MCS technique for stochastic structural response sensitivity", *Comput. Methods Appl. Mech. Eng.* **191**:49–50 (2002), 5631–5645.

[Cecchi and Sab 2009] A. Cecchi and K. Sab, "Discrete and continuous models for in plane loaded random elastic brickwork", *Eur. J. Mech. A Solids* **28**:3 (2009), 610–625.

[Chakraborty and Gopalakrishnan 2004] A. Chakraborty and S. Gopalakrishnan, "A higher-order spectral element for wave propagation analysis in functionally graded materials", *Acta Mech.* **172**:1–2 (2004), 17–43.

[Decker 1991] K. M. Decker, "The Monte Carlo method in science and engineering: theory and application", *Comput. Methods Appl. Mech. Eng.* **89**:1-3 (1991), 463–483.

[Doyle 1997] J. F. Doyle, *Wave propagation in structures: spectral analysis using fast discrete Fourier transforms*, Springer, New York, 1997.

[Ghanem and Spanos 2003] R. G. Ghanem and P. D. Spanos, *Stochastic finite elements: a spectral approach*, Dover, Minneola, NY, 2003.

[Gopalakrishnan et al. 2008] S. Gopalakrishnan, A. Chakraborty, and D. R. Mahapatra, *Spectral finite element method: wave propagation, diagnostics and control in anisotropic and inhomogenous structures*, Springer, London, 2008.

[Horr and Safi 2003] A. M. Horr and M. Safi, "Full dynamic analysis of offshore platform structures using exact Timoshenko pipe element", *J. Offshore Mech. Arct. Eng.* **125**:3 (2003), 168–175.

[James 1980] F. James, "Monte Carlo theory and practice", *Rep. Prog. Phys.* **43**:9 (1980), 1146–1189.

[Kleiber and Hien 1992] M. Kleiber and T. D. Hien, *The stochastic finite element method: basic perturbation technique and computer implementation*, Wiley, Chichester, UK, 1992.

[Lepage 2006] S. Lepage, *Stochastic finite element method for the modeling of thermoelastic damping in micro-resonators*, Ph.D. thesis, Université de Liège, 2006, Available at http://www.ltas-vis.ulg.ac.be/cmsms/uploads/File/Lepage_PhD.pdf.

[Li and Chen 2006] J. Li and J. B. Chen, "The probability density evolution method for dynamic response analysis of non-linear stochastic structures", *Int. J. Numer. Methods Eng.* **65**:6 (2006), 882–903.

[Liu et al. 1986a] W. K. Liu, T. Belytschko, and A. Mani, "Probabilistic finite elements for nonlinear structural dynamics", *Comput. Methods Appl. Mech. Eng.* **56**:1 (1986), 61–81.

[Liu et al. 1986b] W. K. Liu, T. Belytschko, and A. Mani, "Random field finite elements", *Int. J. Numer. Methods Eng.* **23**:10 (1986), 1831–1845.

[Martin et al. 1994] M. A. Martin, S. Gopalakrishnan, and J. F. Doyle, "Wave propagation in multiply connected deep waveguides", *J. Sound Vib.* **174**:4 (1994), 521–538.

[Mindlin and Herrmann 1952] R. D. Mindlin and G. Herrmann, "A one dimensional theory of compressional waves in an elastic rod", pp. 187–191 in *Proceedings of the First U.S. National Congress of Applied Mechanics* (Chicago, 1951), American Soc. Mech. Eng., New York, 1952.

[Nag et al. 2003] A. Nag, D. R. Mahapatra, S. Gopalakrishnan, and T. S. Sankar, "A spectral finite element with embedded delamination for modeling of wave scattering in composite beams", *Compos. Sci. Technol.* **63**:15 (2003), 2187–2200.

[Ostachowicz 2005] W. Ostachowicz, "Elastic wave propagation development for structural health monitoring", pp. 275–286 in *Mechanics of the 21st century: Proceedings of the 21st International Congress of Theoretical and Applied Mechanics* (Warsaw, Poland, 2004), Springer, Dordrecht, 2005.

[Pardoen 1989] G. C. Pardoen, "Effect of delamination on the natural frequencies of composite laminates", *J. Compos. Mater.* **23**:12 (1989), 1200–1215.

[Schueller 2001] G. I. Schueller, "Computational stochastic mechanics-recent advances", *Comput. Struct.* **79**:22-25 (2001), 2225–2234.

[Shinozuka 1972] M. Shinozuka, "Monte Carlo solution of structural dynamics", *Comput. Struct.* **2**:5-6 (1972), 855–874.

[Spanos and Zeldin 1998] P. D. Spanos and B. A. Zeldin, "Monte Carlo treatment of random fields: a broad perspective", *Appl. Mech. Rev.* (*ASME*) **51**:3 (1998), 219–237.

[Stefanou 2009] G. Stefanou, "The stochastic finite element method: past, present and future", *Comput. Methods Appl. Mech. Eng.* **198**:9-12 (2009), 1031–1051.

[Vinckenroy and De Wilde 1995] G. V. Vinckenroy and W. P. De Wilde, "The use of Monte Carlo techniques in statistical finite element methods for the determination of the structural behaviour of composite materials structural components", *Compos. Struct.* **32**:1-4 (1995), 247–253.

Received 28 Jul 2009. Revised 1 Jan 2010. Accepted 14 Jan 2010.

V. AJITH: ajith@aero.iisc.ernet.in
Department of Aerospace Engineering, Indian Institute of Science, Bangalore 560012, India

S. GOPALAKRISHNAN: krishnan@aero.iisc.ernet.in
Department of Aerospace Engineering, Indian Institute of Science, Bangalore 560012, India
http://www.aero.iisc.ernet.in/krishnan

JOURNAL OF MECHANICS OF MATERIALS AND STRUCTURES

http://www.jomms.org

Founded by Charles R. Steele and Marie-Louise Steele

EDITORS

CHARLES R. STEELE	Stanford University, U.S.A.
DAVIDE BIGONI	University of Trento, Italy
IWONA JASIUK	University of Illinois at Urbana-Champaign, U.S.A.
YASUHIDE SHINDO	Tohoku University, Japan

EDITORIAL BOARD

H. D. BUI	École Polytechnique, France
J. P. CARTER	University of Sydney, Australia
R. M. CHRISTENSEN	Stanford University, U.S.A.
G. M. L. GLADWELL	University of Waterloo, Canada
D. H. HODGES	Georgia Institute of Technology, U.S.A.
J. HUTCHINSON	Harvard University, U.S.A.
C. HWU	National Cheng Kung University, R.O. China
B. L. KARIHALOO	University of Wales, U.K.
Y. Y. KIM	Seoul National University, Republic of Korea
Z. MROZ	Academy of Science, Poland
D. PAMPLONA	Universidade Católica do Rio de Janeiro, Brazil
M. B. RUBIN	Technion, Haifa, Israel
A. N. SHUPIKOV	Ukrainian Academy of Sciences, Ukraine
T. TARNAI	University Budapest, Hungary
F. Y. M. WAN	University of California, Irvine, U.S.A.
P. WRIGGERS	Universität Hannover, Germany
W. YANG	Tsinghua University, P.R. China
F. ZIEGLER	Technische Universität Wien, Austria

PRODUCTION

PAULO NEY DE SOUZA	Production Manager
SHEILA NEWBERY	Senior Production Editor
SILVIO LEVY	Scientific Editor

Cover design: Alex Scorpan — Cover photo: Mando Gomez, www.mandolux.com

See inside back cover or http://www.jomms.org for submission guidelines.

JoMMS (ISSN 1559-3959) is published in 10 issues a year. The subscription price for 2010 is US $500/year for the electronic version, and $660/year (+$60 shipping outside the US) for print and electronic. Subscriptions, requests for back issues, and changes of address should be sent to Mathematical Sciences Publishers, Department of Mathematics, University of California, Berkeley, CA 94720–3840.

JoMMS peer-review and production is managed by EditFLOW™ from Mathematical Sciences Publishers.

PUBLISHED BY

mathematical sciences publishers

http://www.mathscipub.org

A NON-PROFIT CORPORATION

Typeset in LaTeX

©Copyright 2010. Journal of Mechanics of Materials and Structures. All rights reserved.

Journal of Mechanics of Materials and Structures

Volume 5, No. 4 April 2010

1559-3959(2010)5:4;1-E